J|A|C|S ARTICLES

Published on Web 02/01/2010

Conformational Flexibility of Y145Stop Human Prion Protein Amyloid Fibrils Probed by Solid-State Nuclear Magnetic Resonance Spectroscopy

Jonathan J. Helmus,[†] Krystyna Surewicz,[‡] Witold K. Surewicz,[‡] and Christopher P. Jaroniec*,[†]

Department of Chemistry, The Ohio State University, Columbus, Ohio 43210, and Department of Physiology and Biophysics, Case Western Reserve University, Cleveland, Ohio 44106

Received November 19, 2009; E-mail: jaroniec@chemistry.ohio-state.edu

Abstract: Amyloid aggregates of a C-truncated Y145Stop mutant of human prion protein, huPrP23−144, associated with a heritable amyloid angiopathy, have previously been shown to contain a compact, relatively rigid, and β-sheet-rich ~30-residue amyloid core near the C-terminus under physiologically relevant conditions. In contrast, the remaining huPrP23−144 residues display considerable conformational dynamics, as evidenced by the absence of corresponding signals in cross-polarization (CP)-based solid-state NMR (SSNMR) spectra under ambient conditions and their emergence in analogous spectra recorded at low temperature on frozen fibril samples. Here, we present the direct observation of residues comprising the flexible N-terminal domain of huPrP23−144 amyloid by using 2D *J*-coupling-based magic-angle spinning (MAS) SSNMR techniques. Chemical shifts for these residues indicate that the N-terminal domain is effectively an ensemble of protein chains with random-coil-like conformations. Interestingly, a detailed analysis of signal intensities in CP-based 3D SSNMR spectra suggests that non-negligible molecular motions may also be occurring on the NMR time scale within the relatively rigid core of huPrP23−144 amyloid. To further investigate this hypothesis, quantitative measurements of backbone dipolar order parameters and transverse spin relaxation rates were performed for the core residues. The observed order parameters indicate that, on the submicrosecond time scale, these residues are effectively rigid and experience only highly restricted and relatively uniform motions similar to those characteristic for well-structured regions of microcrystalline proteins. On the other hand, significant variations in magnitude of transverse spin relaxation rates were noted for residues present at different locations within the core region and correlated with observed differences in spectral intensities. While interpreted only qualitatively at the present time, the extent of the observed variations in transverse relaxation rates is consistent with the presence of relatively slow, microsecond−millisecond time scale chemical exchange type phenomena within the huPrP23−144 amyloid core.

Introduction

The structural rearrangement of a largely α-helical cellular brain protein, dubbed prion protein or PrP^{C}, to highly organized, β-sheet-rich amyloid-like aggregates, PrP^{Sc}, underlies a class of fatal neurological disorders in mammals, referred to as transmissible spongiform encephalopathies or prion diseases.[1−5] According to the "protein-only" hypothesis,[6,7] the misfolded PrP^{Sc} isoform itself acts as the infectious agent that self-propagates by a mechanism involving binding to PrP^{C} and templating its conformational conversion to PrP^{Sc} state. The finding that infectious PrP^{Sc} particles can be generated in vitro,[8−10] combined with discoveries of prion-like protein conformation-based inheritance phenomena in yeast and other fungi,[11−13] have provided important data in support of the notion that proteins alone can function as self-replicating infectious agents. While most recent evidence points to the ability of PrP^{Sc} aggregates to adopt a spectrum of molecular conformations as being a key determinant of prion propagation, the molecular mechanisms of prion and amyloid conformational inheritance and infectivity remain generally poorly understood at the atomic level.[14−16]

[†] The Ohio State University.
[‡] Case Western Reserve University.

(1) Prusiner, S. B. *Proc. Natl. Acad. Sci. U.S.A.* **1998**, *95*, 13363–13383.
(2) Collinge, J. *Annu. Rev. Neurosci.* **2001**, *24*, 519–550.
(3) Caughey, B.; Chesebro, B. *Adv. Virus Res.* **2001**, *56*, 277–311.
(4) Aguzzi, A.; Polymenidou, M. *Cell* **2004**, *116*, 313–327.
(5) Weissmann, C. *Nat. Rev. Microbiol.* **2004**, *2*, 861–871.
(6) Griffith, J. S. *Nature* **1967**, *215*, 1043–1044.
(7) Prusiner, S. B. *Science* **1982**, *216*, 136–144.
(8) Legname, G.; Baskakov, I. V.; Nguyen, H. O.; Riesner, D.; Cohen, F. E.; DeArmond, S. J.; Prusiner, S. B. *Science* **2004**, *305*, 673–676.
(9) Castilla, J.; Saa, P.; Hetz, C.; Soto, C. *Cell* **2005**, *121*, 195–206.
(10) Deleault, N. R.; Harris, B. T.; Rees, J. R.; Supattapone, S. *Proc. Natl. Acad. Sci. U.S.A.* **2007**, *104*, 9741–9746.
(11) Uptain, S. M.; Lindquist, S. *Annu. Rev. Microbiol.* **2002**, *56*, 703–741.
(12) Chien, P.; Weissman, J. S.; DePace, A. H. *Annu. Rev. Biochem.* **2004**, *73*, 617–656.
(13) Wickner, R. B.; Edskes, H. K.; Roberts, B. T.; Baxa, U.; Pierce, M. M.; Ross, E. D.; Brachmann, A. *Genes Dev.* **2004**, *18*, 470–485.
(14) Collinge, J.; Clarke, A. R. *Science* **2007**, *318*, 930–936.

Previous studies by us and others have demonstrated that certain features of mammalian prion conversion to the amyloid state can be conveniently modeled in vitro, using a C-truncated Y145Stop human PrP variant, huPrP23−144, linked to the pathogenesis of a hereditary cerebral amyloid angiopathy.[17−19] Recombinant PrP23−144 is readily converted under physiologically relevant buffer conditions from soluble monomeric form to amyloid fibrils, and this conversion reaction occurs in a nucleation-dependent, autocatalytic manner.[20,21] Although PrP23−144 fibrils have not been shown to be infectious in vivo, this simple system provides a convenient model in vitro for studying some of the most fundamental aspects of mammalian prion propagation including the phenomena of prion strains and species barriers.[22,23] While a systematic series of biochemical and biophysical studies carried out using several homologous mammalian PrP23−144 sequences[22,23] established that seeding specificities of PrP23−144 amyloid are a consequence of the unique conformational properties of different amyloid strains, the methods used in this analysis were of inherently low resolution, precluding the full molecular-level understanding of these phenomena.

To elucidate the detailed structural basis of PrP23−144 strains and seeding specificities, we have recently commenced the characterization of PrP23−144 amyloid fibrils by using high-resolution multidimensional magic-angle spinning (MAS) solid-state nuclear magnetic resonance (SSNMR) techniques. Surprisingly, our initial studies revealed that human PrP23−144 amyloid contains a highly compact, relatively rigid, and β-sheet-rich core region of only ∼30 amino acids (aa) located near the C-terminus.[24] Concurrently, the remaining residues, corresponding primarily to the large N-terminal domain (aa ∼23−111), exhibit significant conformational flexibility within the fibril lattice. The latter conclusion was based on results of variable-temperature SSNMR studies, which showed that signals for the vast majority of huPrP23−144 residues were "invisible" in conventional cross-polarization[25] (CP)-based SSNMR spectra recorded above −20 °C due to the effective motional averaging of nuclear magnetic dipole−dipole couplings, but could be detected at lower temperatures upon freezing the fibrils.

Here, we extend our SSNMR analysis of the conformational flexibility of huPrP23−144 amyloid by detecting directly, at ambient conditions, the highly dynamic huPrP23−144 segments using *J*-coupling-based MAS SSNMR methods, and probing the molecular motions occurring on the NMR time scale within the relatively rigid amyloid core domain using site-resolved SSNMR measurements of backbone dipolar order parameters and transverse spin relaxation rate constants. Altogether, these studies reveal that huPrP23−144 fibrils share common features with other amyloid fibrils composed of intact protein molecules including α-synuclein,[26] tau,[27,28] and fungal prion protein HET-s,[29−32] and highlight the structural and dynamic complexities inherent to protein assemblies of this type.

Experimental Section

Preparation of ^{13}C,^{15}N-Labeled huPrP23−144 Amyloid Fibrils. Uniformly ^{13}C,^{15}N-labeled huPrP23−144 was overexpressed in *Escherichia coli* and purified as described previously.[24] Lyophylized huPrP23−144 was dissolved in ultrapure water at a concentration of 5 mg/mL (∼0.4 mM). Fibril formation was initiated by addition of pH 6.4 potassium phosphate buffer to a final concentration of 50 mM and was allowed to proceed to completion overnight at 25 °C. Fibrils were routinely characterized by atomic force microscopy to confirm sample homogeneity,[23,24] pelleted by low-speed centrifugation, washed with several aliquots of 50 mM pH 6.4 potassium phosphate buffer, and centrifuged directly into a 3.2 mm limited-speed (36 μL) Varian (Palo Alto, CA) zirconia rotor. The rotor was sealed using custom-made spacers (Revolution NMR, Fort Collins, CO) to prevent sample dehydration during experiments. The final SSNMR sample contained ∼12 mg of ^{13}C,^{15}N-labeled huPrP23−144 fibrils.

Solid-State NMR Spectroscopy. NMR experiments were performed at 11.7 T (499.8 MHz for ^{1}H, 125.7 MHz for ^{13}C, and 50.6 MHz for ^{15}N), using a three-channel Varian spectrometer equipped with 3.2 mm triple-resonance T3 and BioMAS probes[33] in ^{1}H−^{13}C−^{15}N configuration. All experiments employed MAS rates, $\omega_r/2\pi$, in the ∼9−11 kHz regime, and temperatures in the 0−30 °C range, as indicated in the text and figure captions. Sample spinning rates were actively regulated to ca. ±3 Hz using a Varian MAS control unit, and sample temperatures were controlled by a stream of dry compressed air, delivered to the sample using a variable-temperature (VT) stack at a flow rate of 30 L/min. Note that all temperatures listed in this Article consistently refer to the VT gas temperature at the sample; the actual average sample temperatures were ∼5 °C higher due to frictional heating as determined by lead nitrate calibration.[34]

The pulse sequence diagrams for all experiments used in this study are shown in Figures S1−S3 of the Supporting Information, and the key experimental parameters are summarized below (see figure captions for additional details). Typical ^{1}H, ^{13}C, and ^{15}N 90° pulse lengths were 2.5, 5.0, and 5.0 μs, respectively, and ∼70 kHz two pulse phase modulated (TPPM) proton decoupling[35] was applied during the chemical shift evolution periods unless indicated

(15) Aguzzi, A.; Sigurdson, C.; Heikenwaelder, M. *Annu. Rev. Pathol.* **2008**, *3*, 11–40.
(16) Cobb, N. J.; Surewicz, W. K. *Biochemistry* **2009**, *48*, 2574–2585.
(17) Surewicz, W. K.; Jones, E. M.; Apetri, A. C. *Acc. Chem. Res.* **2006**, *39*, 654–662.
(18) Kitamoto, T.; Iizuka, R.; Tateishi, J. *Biochem. Biophys. Res. Commun.* **1993**, *192*, 532–537.
(19) Ghetti, B. *Proc. Natl. Acad. Sci. U.S.A.* **1996**, *93*, 744–748.
(20) Kundu, B.; Maiti, N. R.; Jones, E. M.; Surewicz, K. A.; Vanik, D. L.; Surewicz, W. K. *Proc. Natl. Acad. Sci. U.S.A.* **2003**, *100*, 12069–12074.
(21) Moore, R. A.; Herzog, C.; Errett, J.; Kocisko, D. A.; Arnold, K. M.; Hayes, S. F.; Priola, S. A. *Protein Sci.* **2006**, *15*, 609–619.
(22) Vanik, D. L.; Surewicz, K. A.; Surewicz, W. K. *Mol. Cell* **2004**, *14*, 139–145.
(23) Jones, E. M.; Surewicz, W. K. *Cell* **2005**, *121*, 63–72.
(24) Helmus, J. J.; Surewicz, K.; Nadaud, P. S.; Surewicz, W. K.; Jaroniec, C. P. *Proc. Natl. Acad. Sci. U.S.A.* **2008**, *105*, 6284–6289.
(25) Pines, A.; Gibby, M. G.; Waugh, J. S. *J. Chem. Phys.* **1973**, *59*, 569–590.
(26) Heise, H.; Hoyer, W.; Becker, S.; Andronesi, O. C.; Riedel, D.; Baldus, M. *Proc. Natl. Acad. Sci. U.S.A.* **2005**, *102*, 15871–15876.
(27) Sillen, A.; Wieruszeski, J. M.; Leroy, A.; Ben Younes, A.; Landrieu, I.; Lippens, G. *J. Am. Chem. Soc.* **2005**, *127*, 10138–10139.
(28) Andronesi, O. C.; von Bergen, M.; Biernat, J.; Seidel, K.; Griesinger, C.; Mandelkow, E.; Baldus, M. *J. Am. Chem. Soc.* **2008**, *130*, 5922–5928.
(29) Siemer, A. B.; Arnold, A. A.; Ritter, C.; Westfeld, T.; Ernst, M.; Riek, R.; Meier, B. H. *J. Am. Chem. Soc.* **2006**, *128*, 13224–13228.
(30) Wasmer, C.; Lange, A.; Van Melckebeke, H.; Siemer, A. B.; Riek, R.; Meier, B. H. *Science* **2008**, *319*, 1523–1526.
(31) Lange, A.; Gattin, Z.; Van Melckebeke, H.; Wasmer, C.; Soragni, A.; van Gunsteren, W. F.; Meier, B. H. *ChemBioChem* **2009**, *10*, 1657–1665.
(32) Wasmer, C.; Schütz, A.; Loquet, A.; Buhtz, C.; Greenwald, J.; Riek, R.; Böckmann, A.; Meier, B. H. *J. Mol. Biol.* **2009**, *394*, 119–127.
(33) Stringer, J. A.; Bronnimann, C. E.; Mullen, C. G.; Zhou, D. H. H.; Stellfox, S. A.; Li, Y.; Williams, E. H.; Rienstra, C. M. *J. Magn. Reson.* **2005**, *173*, 40–48.
(34) Bielecki, A.; Burum, D. P. *J. Magn. Reson., Ser. A* **1995**, *116*, 215–220.
(35) Bennett, A. E.; Rienstra, C. M.; Auger, M.; Lakshmi, K. V.; Griffin, R. G. *J. Chem. Phys.* **1995**, *103*, 6951–6957.

otherwise. 2D refocused INEPT experiments[36,37] (Figure S1A) recorded at 11.111 kHz MAS rate were used to obtain $^{1}H-^{13}C$ and $^{1}H-^{15}N$ correlation spectra containing signals from the most flexible segments of huPrP23−144 fibrils. The total durations of $^{1}H-^{13}C$ and $^{1}H-^{15}N$ magnetization transfer periods were 4.4 and 8.0 ms, respectively. The CTUC−COSY scheme,[38] preceded by either $^{1}H-^{13}C$ cross-polarization (Figure S1B) or refocused INEPT (Figure S1C), was used at 11.111 kHz MAS rate to record 2D $^{13}C^{\alpha}-^{13}C'$ spectra with correlations arising exclusively from the rigid amyloid core residues or the flexible segments of huPrP23−144 fibrils, respectively. The total duration of the $^{13}C-^{13}C$ mixing period was 18 ms, during which ∼100 kHz TPPM ^{1}H decoupling was applied.

The effective $^{1}H^{N}-^{15}N$ and $^{1}H^{\alpha}-^{13}C^{\alpha}$ one-bond dipolar couplings for residues in the amyloid core region of huPrP23−144 fibrils were probed at a MAS frequency of 9.470 kHz using 3D dipolar-chemical shift experiments,[39−42] which employed SPECIFIC CP[43] to generate $^{15}N-^{13}C^{\alpha}$ correlations and the T-MREV pulse scheme[41] to achieve simultaneous $^{1}H-^{13}C$ or $^{1}H-^{15}N$ recoupling and $^{1}H-^{1}H$ decoupling (Figure S2A). The T-MREV ^{1}H radiofrequency (RF) field strength was set to 113.6 kHz (corresponding to a 90° ^{1}H pulse length of 2.2 μs), and four T-MREV elements were incorporated into each rotor cycle. The effective $^{15}N-^{13}C^{\alpha}$ and $^{15}N-^{13}C'$ one-bond dipolar couplings were determined at 11.111 kHz MAS rate using a 3D band-selective TEDOR scheme[44] (Figure S2B). The $^{13}C^{\alpha}-^{13}C'$ *J*-decoupling during the $^{15}N-^{13}C^{\alpha}$ or $^{15}N-^{13}C'$ recoupling periods[44−47] was achieved using frequency selective ^{13}C r-SNOB pulses[48,49] with duration 360 μs, applied in the $^{13}C^{\alpha}$ (∼54 ppm) or $^{13}C'$ spectral region (∼174 ppm), respectively. The 180° ^{15}N recoupling pulse train was applied at a field strength of ∼28 kHz and phase cycled according to the *xy*-4 scheme.[50] TPPM ^{1}H decoupling at a RF field strength of ∼100 kHz was applied throughout the $^{15}N-^{13}C$ dipolar mixing and ^{15}N chemical shift evolution periods.

Measurements of selected ^{1}H, ^{13}C, and ^{15}N transverse relaxation rate constants, $R_{1\rho}$ and R_2, were performed at 11.111 kHz MAS by combining the 2D $^{15}N-^{13}C^{\alpha}$ SPECIFIC CP scheme with an evolution period, during which appropriate NMR coherences were allowed to decay (Figure S3). For $^{1}H^{N}$ $R_{1\rho}$ measurements, a ∼90 kHz spin-lock field was applied on the ^{1}H channel prior to $^{1}H-^{15}N$ CP. For the ^{15}N and $^{13}C^{\alpha}$ $R_{1\rho}$ measurements, ∼28 kHz spin-lock fields (satisfying the condition $\omega_{RF} \approx 2.5\omega_r$) were applied on ^{15}N and ^{13}C channels, respectively, with concurrent ∼100 kHz ^{1}H continuous wave (CW) decoupling. These RF field settings were optimized to avoid ^{15}N and ^{13}C dipolar and chemical shift rotary resonance conditions[51] and $^{15}N/^{13}C-^{1}H$ dipolar recoupling.[52] For the ^{15}N R_2 measurements, a spin−echo period consisting of a single 180° ^{15}N pulse with concurrent ∼70 kHz TPPM ^{1}H decoupling was inserted immediately prior to ^{15}N chemical shift evolution.

To minimize potential long-term fluctuations of peak intensities during extended 3D SSNMR experiments designed to measure dipolar or relaxation trajectories, the corresponding pulse sequences were implemented with: (i) a constant duty factor by appending additional RF pulses on the appropriate channels following signal acquisition, and (ii) sampling the dipolar and relaxation dimension increments in an interleaved fashion, as the innermost loops of the 3D data sets.

Data Processing and Simulations. All NMR spectra were processed and analyzed using the NMRPipe/NMRDraw software package,[53] where a typical 3D NMR experiment designed to measure dipolar couplings or relaxation rates in site-resolved fashion consists of a series of 2D $^{15}N-^{13}C$ correlation spectra recorded for different values of a dipolar evolution time, τ_{mix}, or relaxation delay, τ (see pulse schemes in Figures S2 and S3). For each 2D $^{15}N-^{13}C$ spectrum in the series, the residue-specific cross-peak volumes were obtained using in-house Python scripts by summing up spectral intensities within integration boxes with dimensions corresponding to approximately the full peak width at half-maximum along the ^{15}N and ^{13}C frequency axes. Note that for each cross-peak, the integration box dimensions were defined using the 2D spectrum in the series having the highest overall intensity, and subsequently used to integrate each spectrum in the series. This procedure yielded the cross-peak volumes and their uncertainties, σ, according to $\sigma = (N)^{1/2} \cdot \sigma_{noise}$, where N is the number of spectral intensities present within the box limits and summed up to obtain the cross-peak volume, and σ_{noise} is the estimated experimental noise that corresponds effectively to the root-mean-squared (rms) noise obtained within NMRDraw by examining noise distributions in empty regions of the spectra.

Simulations of the $^{1}H^{N}-^{15}N$ and $^{1}H^{\alpha}-^{13}C^{\alpha}$ T-MREV dipolar trajectories were carried out in the time-domain using an average Liouvillian approach, described in detail by Hohwy et al.[41] and Rienstra et al.[42] and implemented in FORTRAN. The adjustable fit parameters included: (1) the magnitude of the scaled one-bond dipolar coupling between the heavy atom, ^{13}C or ^{15}N, and the directly bonded ^{1}H, (2) the average proton coherence decay rate, Γ_2, and (3) an overall amplitude scaling factor. Moreover, to obtain the most accurate estimate of the one-bond dipolar couplings of interest, the simulation model also took into account two additional, weaker dipolar couplings between the heavy atom and distant protons, which were not varied during the simulation.[41,42]

Simulations of the $^{15}N-^{13}C^{\alpha}$ and $^{15}N-^{13}C'$ band-selective TEDOR dipolar trajectories were carried out in the time-domain using an average Hamiltonian approach described previously,[44,47] implemented in FORTRAN. The adjustable fit parameters included: (1) the magnitude of the scaled one-bond $^{15}N-^{13}C$ dipolar coupling, (2) the ^{13}C transverse relaxation rate, modeled as a single exponential decay, and (3) an overall amplitude scaling factor. In addition, the simulation model included: the passive dipolar coupling between the ^{13}C spin and the next nearest ^{15}N nucleus, the effects of finite ^{15}N pulses during TEDOR mixing,[54] and for the $^{15}N-^{13}C^{\alpha}$ experiment for all residues except glycine, the ∼35 Hz $^{13}C^{\alpha}-^{13}C^{\beta}$ *J*-coupling not refocused by the shaped pulse.

The ^{1}H, ^{13}C, and ^{15}N transverse relaxation rate constants were extracted by fitting cross-peak trajectories as a function of the

(36) Morris, G. A. *J. Am. Chem. Soc.* **1980**, *102*, 428–429.
(37) Andronesi, O. C.; Becker, S.; Seidel, K.; Heise, H.; Young, H. S.; Baldus, M. *J. Am. Chem. Soc.* **2005**, *127*, 12965–12974.
(38) Chen, L.; Olsen, R. A.; Elliott, D. W.; Boettcher, J. M.; Zhou, D. H.; Rienstra, C. M.; Mueller, L. J. *J. Am. Chem. Soc.* **2006**, *128*, 9992–9993.
(39) Munowitz, M. G.; Griffin, R. G.; Bodenhausen, G.; Huang, T. H. *J. Am. Chem. Soc.* **1981**, *103*, 2529–2533.
(40) Munowitz, M. G.; Griffin, R. G. *J. Chem. Phys.* **1982**, *76*, 2848–2858.
(41) Hohwy, M.; Jaroniec, C. P.; Reif, B.; Rienstra, C. M.; Griffin, R. G. *J. Am. Chem. Soc.* **2000**, *122*, 3218–3219.
(42) Rienstra, C. M.; Hohwy, M.; Mueller, L. J.; Jaroniec, C. P.; Reif, B.; Griffin, R. G. *J. Am. Chem. Soc.* **2002**, *124*, 11908–11922.
(43) Baldus, M.; Petkova, A. T.; Herzfeld, J.; Griffin, R. G. *Mol. Phys.* **1998**, *95*, 1197–1207.
(44) Jaroniec, C. P.; Filip, C.; Griffin, R. G. *J. Am. Chem. Soc.* **2002**, *124*, 10728–10742.
(45) Jaroniec, C. P.; Tounge, B. A.; Rienstra, C. M.; Herzfeld, J.; Griffin, R. G. *J. Am. Chem. Soc.* **1999**, *121*, 10237–10238.
(46) Jaroniec, C. P.; Tounge, B. A.; Herzfeld, J.; Griffin, R. G. *J. Am. Chem. Soc.* **2001**, *123*, 3507–3519.
(47) Helmus, J. J.; Nadaud, P. S.; Hofer, N.; Jaroniec, C. P. *J. Chem. Phys.* **2008**, *128*, 052314.
(48) Kupce, E.; Boyd, J.; Campbell, I. D. *J. Magn. Reson., Ser. B* **1995**, *106*, 300–303.
(49) Li, Y.; Wylie, B. J.; Rienstra, C. M. *J. Magn. Reson.* **2006**, *179*, 206–216.
(50) Gullion, T.; Baker, D. B.; Conradi, M. S. *J. Magn. Reson.* **1990**, *89*, 479–484.
(51) Oas, T. G.; Griffin, R. G.; Levitt, M. H. *J. Chem. Phys.* **1988**, *89*, 692–695.
(52) Ishii, Y.; Ashida, J.; Terao, T. *Chem. Phys. Lett.* **1995**, *246*, 439–445.
(53) Delaglio, F.; Grzesiek, S.; Vuister, G. W.; Zhu, G.; Pfeifer, J.; Bax, A. *J. Biomol. NMR* **1995**, *6*, 277–293.
(54) Jaroniec, C. P.; Tounge, B. A.; Rienstra, C. M.; Herzfeld, J.; Griffin, R. G. *J. Magn. Reson.* **2000**, *146*, 132–139.

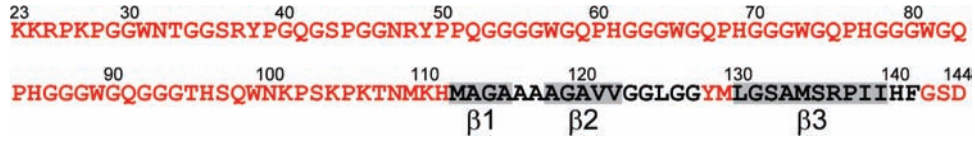

Figure 1. Amino acid sequence of huPrP23−144. Residues in the relatively rigid amyloid core region are shown in black font, with predicted β-strand segments highlighted by gray rectangles.[24] Residues displaying significant conformational flexibility are shown in red font. A four-residue (Gly-Ser-Asp-Pro) N-terminal extension remaining after thrombin cleavage has been omitted for clarity.

relaxation delay to single exponential decays, with $R_{1\rho}$ or R_2 being the only adjustable fit parameter.

Dipolar Coupling Error Estimation. A Monte Carlo approach, analogous to that described by Rienstra et al.,[42] was used to obtain the best estimates and uncertainties of the one-bond $^{1}H^{N}-^{15}N$, $^{1}H^{\alpha}-^{13}C^{\alpha}$, $^{15}N-^{13}C^{\alpha}$, and $^{15}N-^{13}C'$ dipolar couplings. Briefly, the simulated dipolar trajectory that gave the best fit to the corresponding experimental trajectory was used to generate a set of 5000 synthetic dipolar trajectories. This was accomplished by adding to each time point of the best-fit simulation a random amount of noise drawn from a Gaussian distribution with the standard deviation, σ, given by the noise level obtained from NMR spectra as described above. Each synthetic trajectory was subsequently refit with the same simulation model yielding a set of 5000 dipolar couplings used to form a distribution (see Figures S4−S7 for examples of representative distributions). The best estimate and uncertainty of the dipolar coupling corresponded to the average value and standard deviation of this distribution, respectively. To minimize the computational time associated with the Monte Carlo procedure, extensive grids of simulated dipolar trajectories covering large ranges of the fitting parameters were constructed and repeatedly used to fit all synthetic trajectories.

Results and Discussion

Direct Detection of Highly Flexible Segments of huPrP23−144 Amyloid. Our initial solid-state NMR analysis of huPrP23−144 fibrils identified the presence of a relatively rigid and highly ordered amyloid core region encompassing ~30 residues near the C-terminus (Figure 1).[24] The NMR chemical shifts indicate that the majority of these core residues adopt a β-strand conformation. Remarkably, most of the huPrP23−144 sequence, corresponding primarily to N-terminal amino acids 23−111, was "invisible" in conventional SSNMR experiments performed at temperatures higher than −20 °C due to the motional averaging of magnetic dipole−dipole couplings required for efficient magnetization transfer via cross-polarization. On the other hand, these highly flexible residues could be detected by CP-based SSNMR methods at ca. −30 °C on frozen samples, where the major protein backbone motions in huPrP23−144 fibrils appear to be effectively quenched.[24] Here, we extend our analysis of the mobile huPrP23−144 amyloid segments by using solution-state NMR type (i.e., *J*-coupling based) techniques applied under MAS conditions. Unlike dipolar couplings, *J*-coupling interactions have a nonzero isotropic component and can drive efficient homo- and heteronuclear magnetization transfers in solids even in the presence of significant conformational dynamics. This permits the direct observation of highly flexible domains in immobilized proteins, provided that the relaxation of NMR coherences is sufficiently slow.[26−29,37]

Figure 2 shows $^{1}H-^{13}C$ and $^{1}H-^{15}N$ chemical shift correlation spectra of huPrP23−144 fibrils recorded at ~11 kHz MAS using a 2D refocused INEPT scheme[36,37] (Figure S1A). These spectra were recorded at 30 °C, where the relaxation of ^{1}H, ^{13}C, and ^{15}N coherences is attenuated relative to 0 °C, resulting in a higher INEPT transfer efficiency. Note that our previous studies confirm that the huPrP23−144 amyloid core remains highly ordered at all temperatures between −30 and 30 °C.[24] The $^{1}H-^{13}C$ correlation spectrum (Figure 2A) contains a multitude of intense resonances in the aliphatic and aromatic

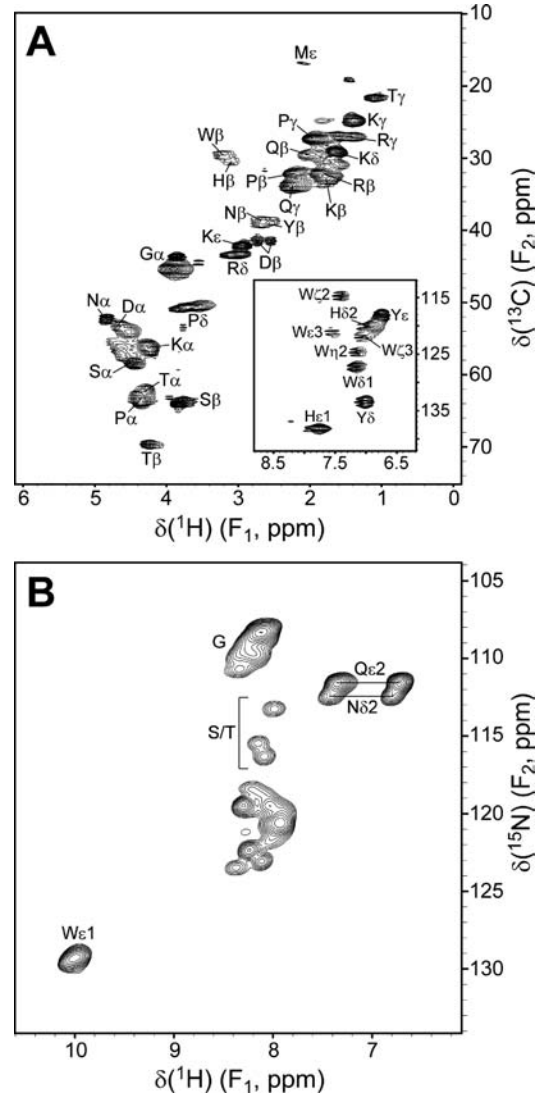

Figure 2. Two-dimensional $^{1}H-^{13}C$ (A) and $^{1}H-^{15}N$ (B) correlation spectra of huPrP23−144 fibrils recorded at 30 °C and 11.111 kHz MAS rate. Refocused INEPT[36] with a total duration of 4.4 or 8.0 ms was used to transfer magnetization from ^{1}H to ^{13}C or ^{15}N, respectively. ^{1}H chemical shift evolution was achieved in a semiconstant time manner[58] (Figure S1A). Spectra were recorded as follows: (A) 360* (t_1, ^{1}H) × 2000* (t_2, ^{13}C) data matrix with acquisition times of 18 ms (t_1) and 40 ms (t_2) and a total measurement time of 24 h; (B) 360* (t_1, ^{1}H) × 2000* (t_2, ^{15}N) data matrix with acquisition times of 18 ms (t_1) and 40 ms (t_2) and a total measurement time of 72 h. Cross-peaks are drawn with the lowest contour at 20 times the rms noise level. Tentative assignments based on average chemical shift values in the BioMagResBank[57] are indicated in the spectra (see Table S1).

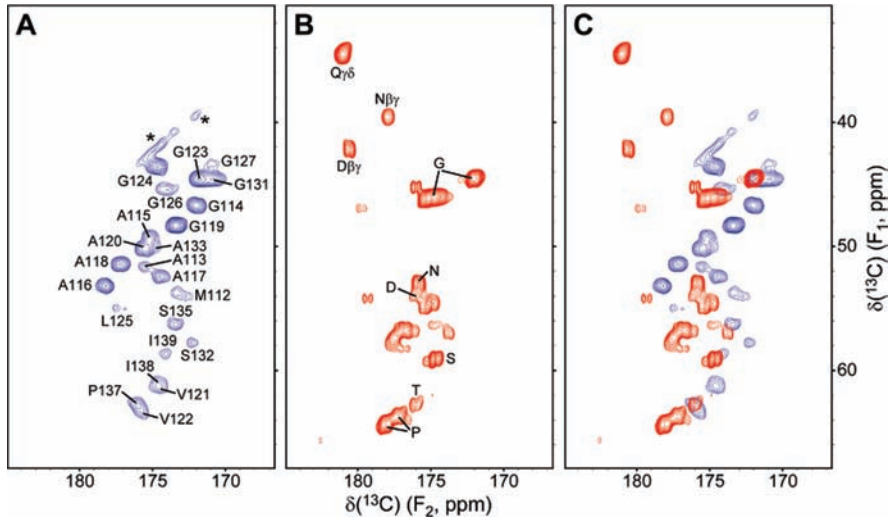

Figure 3. 2D $^{13}C^{\alpha}-^{13}C'$ CTUC−COSY[38] spectra of huPrP23−144 fibrils recorded at 11.111 kHz MAS rate. (A) Spectrum at 0 °C, with initial ^{13}C magnetization generated using $^{1}H-^{13}C$ CP (Figure S1B). (B) Spectrum at 30 °C, with initial ^{13}C magnetization generated using $^{1}H-^{13}C$ refocused INEPT (Figure S1C). (C) Overlay of CP (blue) and refocused INEPT (red) spectra shown in (A) and (B). Spectra were recorded as follows: (A) 100* (t_1, ^{13}C) × 1000* (t_2, ^{13}C) data matrix with acquisition times of 9 ms (t_1) and 20 ms (t_2) and a total measurement time of 32 h; (B) 100* (t_1, ^{13}C) × 1300* (t_2, ^{13}C) data matrix with acquisition times of 9 ms (t_1) and 26 ms (t_2) and a total measurement time of 12 h. Cross-peaks are drawn with the lowest contour at 10 times the rms noise level. Assignments in (A) are taken from Helmus et al.[24] Spinning sidebands are indicated by asterisks. Tentative assignments in (B) are based on average chemical shift values in the BioMagResBank.[57]

regions, most of which exhibit pronounced $^{13}C-^{13}C$ *J*-splittings in the ^{13}C dimension, indicating the effective motional averaging of $^{13}C-^{1}H$ and $^{1}H-^{1}H$ dipolar couplings. Most important, a number of characteristic correlations that can be attributed only to residues present outside the amyloid core region (e.g., Thr and Trp) are present in this $^{1}H-^{13}C$ spectrum. On the other hand, notably suppressed are correlations involving methyl groups of residues found exclusively in the amyloid core region (Ala, Ile, Leu, and Val); this is primarily due to the rapid relaxation of proton coherences for these relatively rigid residues during the first half of the refocused INEPT sequence.

The $^{1}H-^{15}N$ spectrum (Figure 2B) reveals resonance frequencies of approximately 8.1 ± 0.3 ppm for all detected backbone H^N atoms. Tentative assignments of Gly, Ser, and Thr residues (as well as Asn, Gln, and Trp side-chain correlations) could be made on the basis of their characteristic ^{15}N shifts. Amide proton frequencies in this range are typical of unstructured proteins,[55] indicating that the highly flexible N-terminal domain in huPrP23−144 fibrils resembles an ensemble of largely disordered states with random-coil-like conformations.[56] This is in accord with our previous observations of pronounced inhomogeneous linebroadening for this region of huPrP23−144 in low-temperature CP-based SSNMR spectra.[24] Additional evidence for the dynamic disorder in the N-terminal region of huPrP23−144 is provided by the relatively limited dispersion of resonances in the $^{1}H-^{13}C$ spectrum. Indeed, by assuming a random-coil protein conformation, we were able to tentatively assign most resonances in this spectrum by simply mapping the observed chemical shift values onto the average residue- and site-specific chemical shifts listed in the BioMagResBank database (BMRB, http://www.bmrb.wisc.edu).[57] This analysis, summarized in Table S1 of the Supporting Information, yielded the average shift deviations, $\langle \delta_{obs} - \delta_{BMRB} \rangle$, of −0.02 ± 0.10 ppm for H^{α} and −0.2 ± 0.7 ppm for C^{α}/C^{β}, and allowed us to readily identify correlations corresponding to all amino acid types (Arg, Asn, Asp, Gln, Gly, His, Lys, Met, Pro, Ser, Thr, Trp, and Tyr) present outside the core region of huPrP23−144 amyloid.

To further probe the most flexible segments of huPrP23−144 fibrils, we recorded 2D $^{13}C^{\alpha}-^{13}C'$ correlation spectra (Figure 3), where the initial ^{13}C magnetization was prepared using either $^{1}H-^{13}C$ CP or refocused INEPT and the magnetization transfer between coupled ^{13}C nuclei was mediated by one-bond $^{13}C-^{13}C$ *J*-couplings. The spectrum in Figure 3A was acquired using the CTUC−COSY pulse scheme[38] (Figure S1B), with the $^{13}C-^{13}C$ magnetization transfer preceded by $^{1}H-^{13}C$ CP. Given that substantial $^{1}H-^{13}C$ dipolar couplings are required for efficient CP, this scheme effectively suppresses signals arising from the most flexible regions of huPrP23−144 amyloid. Indeed, this "CP-COSY" $^{13}C-^{13}C$ spectrum contains backbone ^{13}C signals from only the amyloid core residues and is in good agreement with the previously reported 2D $^{13}C-^{13}C$ RF-assisted proton driven spin diffusion spectrum.[24] Figure 3B shows a 2D $^{13}C^{\alpha}-^{13}C'$ spectrum also acquired using a CTUC−COSY-type scheme, but where the initial ^{13}C magnetization was prepared by refocused INEPT instead of CP (Figure S1C). In analogy to the $^{1}H-^{13}C$ and $^{1}H-^{15}N$ spectra in Figure 2, this "INEPT-COSY" experiment filters out signals from the amyloid core region and highlights resonances arising exclusively from the most flexible residues of huPrP23−144 (e.g., Asn, Asp, Gln, and Thr). The chemical shift values observed in this $^{13}C-^{13}C$ spectrum combined with the relatively low spectral resolution further substantiate the notion that the N-terminal domain of huPrP23−144 fibrils is most accurately described as a dynamic, random-coil-like ensemble of protein chains.

Probing the Submicrosecond Time Scale Backbone Dynamics in the Core Region of huPrP23−144 Amyloid. In contrast to the highly flexible random-coil-like N-terminal

(58) Grzesiek, S.; Bax, A. *J. Biomol. NMR* **1993**, *3*, 185–204.
(57) Ulrich, E. L. *Nucleic Acids Res.* **2008**, *36*, D402–D408.
(55) Wüthrich, K. *NMR of Proteins and Nucleic Acids*; Wiley: New York, 1986.
(56) Dinner, A. R.; Sali, A.; Smith, L. J.; Dobson, C. M.; Karplus, M. *Trends Biochem. Sci.* **2000**, *25*, 331–339.

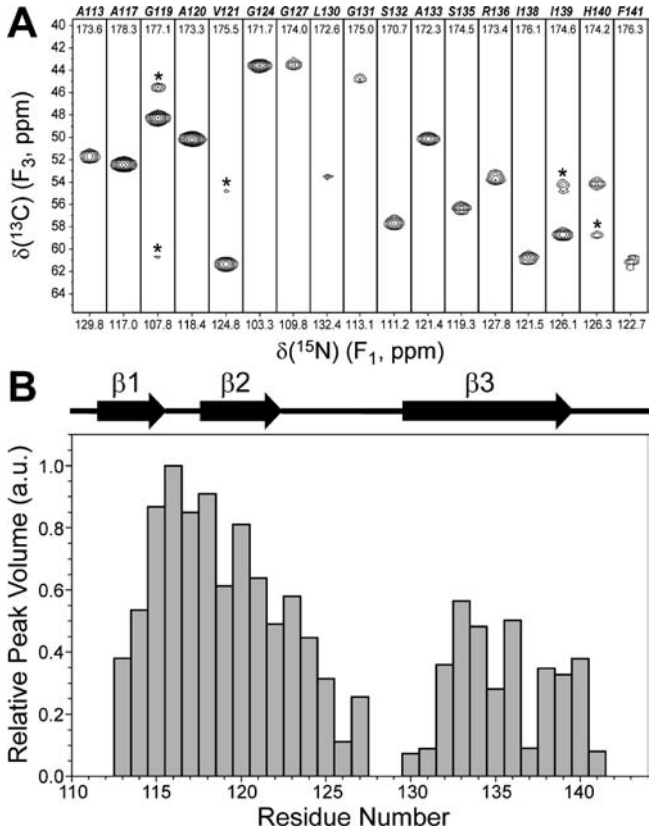

Figure 4. Cross-peak intensities for residues in huPrP23−144 amyloid core. (A) Selected strips from a 3D CONCA spectrum (see Helmus et al.[24] for details of data acquisition). Strips are labeled by residue number according to the ^{15}N frequency, and the ^{13}C′ (F_2) frequency is given inside each strip. Peaks from neighboring spectral planes are marked by asterisks. (B) Relative peak volumes in the 3D CONCA spectrum at 0 °C as a function of residue number. Peak volumes were obtained using NMRPipe/NMRDraw[53] and are given relative to the volume of the most intense correlation (A116).

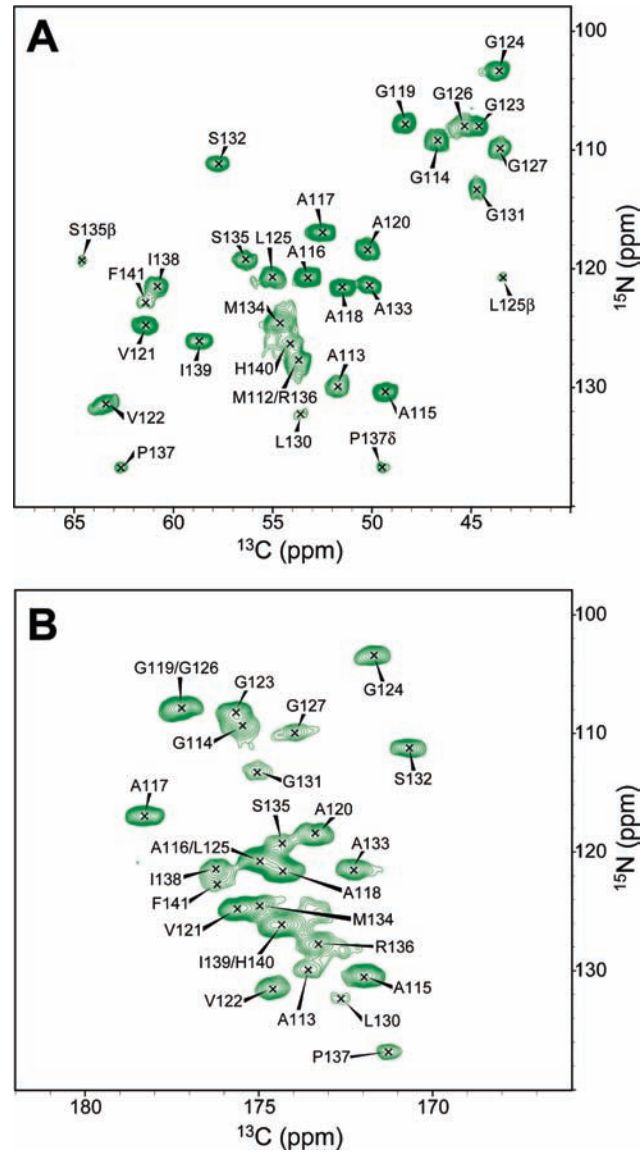

Figure 5. Representative 2D ^{15}N−^{13}C planes from 3D dipolar chemical shift SSNMR experiments on huPrP23−144 amyloid fibrils. (A) 2D ^{15}N−^{13}C$^{\alpha}$ plane from a 3D ^{1}H^{N}−^{15}N T-MREV experiment[41,42] recorded at 0 °C and 9.470 kHz MAS with the dipolar evolution period, τ_{mix}, set to 0 (Figure S2A). The 3D spectrum was recorded in an interleaved fashion for τ_{mix} as a 152* (t_1, ^{15}N) × 1400* (t_2, ^{13}C) × 16 (τ_{mix}, ^{1}H^{N}−^{15}N dipolar coupling) data matrix with acquisition times of 16 ms (t_1), 28 ms (t_2), and 792 μs (τ_{mix}) and a total measurement time of 108 h. (B) 2D ^{15}N−^{13}C′ plane from a 3D band-selective TEDOR experiment[44] recorded at 0 °C and 11.111 kHz MAS with the dipolar evolution period, τ_{mix}, set to 1.44 ms (Figure S2B). The 3D spectrum was recorded in an interleaved fashion for τ_{mix} as a 70* (t_1, ^{15}N) × 1400* (t_2, ^{13}C) × 12 (τ_{mix}, ^{15}N−^{13}C′ dipolar coupling) data matrix with acquisition times of 12.6 ms (t_1), 28 ms (t_2), and 4.32 ms (τ_{mix}) and a total measurement time of 94 h. Cross-peaks in (A) and (B) are drawn with the lowest contour at 7 times the rms noise level. Resonance assignments are based on Helmus et al.,[24] and additional experimental details are provided in the Experimental Section.

domain, the core region of huPrP23−144 amyloid fibrils appears to be generally quite rigid. This relative rigidity permits signals from the core residues to be detected in CP-based solid-state NMR spectra. Nevertheless, the considerable variation of cross-peak intensities in such spectra, as discussed below, suggests that motional phenomena may be present within this core region as well. Here, we describe our analysis of the protein backbone dynamics for the huPrP23−144 core residues.

The fingerprint 2D chemical shift correlation spectra recorded using conventional SSNMR methods (see Figures 3A and 5 for representative ^{13}C−^{13}C and ^{15}N−^{13}C spectra, respectively) reveal that signals arising from residues 112−113 and 140−141 present at the periphery of the amyloid core are visibly attenuated relative to most other cross-peaks. Moreover, missing completely are cross-peaks for residues Y128 and M129 within the core region, while resonances from adjacent residues (e.g., G127, L130, and G131) display notably reduced intensities; similar prior observations formed the basis for the hypothesis that residues 128 and 129 are found in a partially flexible loop within the huPrP23−144 amyloid core.[24] A detailed analysis of peak intensities in analogous 3D SSNMR spectra corroborates these findings and also offers new insights that are not readily apparent from the 2D data sets. In Figure 4, we show representative strips from a 3D ^{13}C′−^{15}N−^{13}C$^{\alpha}$ (CONCA) chemical shift correlation spectrum[24] as well as a plot of cross-peak volume as a function of residue number. These data illustrate that the most rigid part of the huPrP23−144 fibril core (i.e., that characterized by highest cross-peak intensities) corresponds to aa ∼115−120; interestingly, this region spans parts of strands β1 and β2 and contains the short intervening non-β bend. The remaining huPrP23−144 core residues exhibit the following intensity pattern: (i) cross-peaks for residues 121−127 are seen to decrease gradually toward nearly zero intensity, (ii)

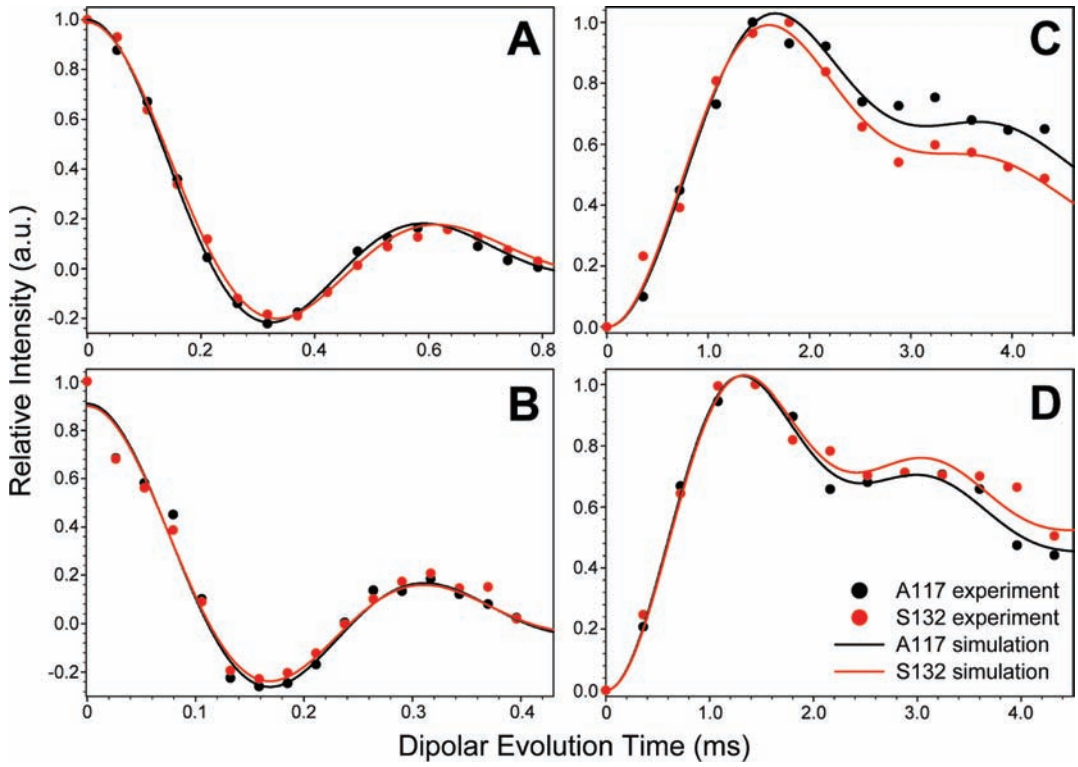

Figure 6. Backbone dipolar couplings in the amyloid core region of huPrP23−144 fibrils. Representative measurements of $^{1}H^{N}-^{15}N$ (A), $^{1}H^{\alpha}-^{13}C^{\alpha}$ (B), $^{15}N-^{13}C^{\alpha}$ (C), and $^{15}N-^{13}C'$ (D) one-bond dipolar couplings are shown for residues A117 and S132 (for $^{15}N-^{13}C'$ couplings, the $^{13}C'$ nucleus corresponds to the preceding residue). The dipolar trajectories were recorded using 3D dipolar-chemical shift correlation SSNMR experiments, as described in the text. For each trajectory, the experimental cross-peak intensity in a 2D $^{15}N-^{13}C^{\alpha}$ (A−C) or $^{15}N-^{13}C'$ (D) correlation spectrum is shown as a function of the dipolar evolution time (circles), and the best-fit simulation is shown as a solid line. Additional trajectories are shown in Figures S4−S7. See the Experimental Section for a detailed description of the simulations.

no cross-peaks are observed for residues 128−129, and very weak signals are seen for residues 130−131 as noted above, and (iii) cross-peaks for residues 132−140 (except for P137, which has no amide proton) have intensities that are on average ~40 ± 10% of those obtained for residues found in the most rigid part of the amyloid core. These findings are consistent with the presence of molecular motions of differing degrees throughout the entire core region of huPrP23−144 fibrils.

To probe for the presence of relatively fast, submicrosecond time scale protein backbone motions,[59,60] we have conducted residue-specific measurements of the magnitudes of one-bond dipolar couplings by using 3D dipolar chemical shift SSNMR methods.[39−42] Such SSNMR measurements have been previously applied to microcrystalline and membrane-associated proteins[61−68] to yield information about backbone dynamics in the form of dipolar order parameters, $\langle S\rangle = d_{IS}^{exp}/d_{IS}^{rigid}$, where d_{IS}^{exp} is the experimentally determined dipolar coupling between nuclear spins I and S, and d_{IS}^{rigid} is the corresponding dipolar coupling in the rigid-lattice limit. These order parameters effectively report on the extent of internuclear bond vector reorientation, where in the absence of dynamics we have $d_{IS}^{exp} = d_{IS}^{rigid}$ and $\langle S\rangle = 1$, while for fully isotropic motion both d_{IS}^{exp} and $\langle S\rangle$ vanish.

Specifically, for each residue in the huPrP23−144 amyloid core, we have measured up to four one-bond dipolar couplings including $^{1}H^{N}-^{15}N$, $^{1}H^{\alpha}-^{13}C^{\alpha}$, $^{15}N-^{13}C^{\alpha}$, and $^{15}N-^{13}C'$. Each type of coupling was measured using a separate 3D SSNMR experiment that consisted of a series of 2D $^{15}N-^{13}C$ correlation spectra recorded as a function of a variable mixing period, during which the appropriate dipolar coupling is reintroduced under MAS while other nuclear spin interactions are largely suppressed (see pulse schemes in Figure S2). Thus, for each residue, these 3D SSNMR experiments yield characteristic cross-peak dephasing ($^{1}H^{N}-^{15}N$ and $^{1}H^{\alpha}-^{13}C^{\alpha}$ couplings) or build-up ($^{15}N-^{13}C^{\alpha}$ and $^{15}N-^{13}C'$ couplings) trajectories, the exact profile of which is determined primarily by the magnitude of the large one-bond dipolar coupling of interest. In Figure 5, we show representative 2D $^{15}N-^{13}C$ planes from experiments designed to measure the $^{1}H^{N}-^{15}N$ (panel A) and $^{15}N-^{13}C'$ (panel B) dipolar couplings to illustrate the resolution and sensitivity of these experiments for huPrP23−144 amyloid fibrils. In Figure 6, we show representative dipolar trajectories for residues A117 and S132,

(59) Palmer, A. G.; Williams, J.; McDermott, A. *J. Phys. Chem.* **1996**, *100*, 13293–13310.
(60) Krushelnitsky, A.; Reichert, D. *Prog. Nucl. Magn. Reson. Spectrosc.* **2005**, *47*, 1–25.
(61) Huster, D.; Xiao, L. S.; Hong, M. *Biochemistry* **2001**, *40*, 7662–7674.
(62) Hong, M.; Yao, X. L.; Jakes, K.; Huster, D. *J. Phys. Chem. B* **2002**, *106*, 7355–7364.
(63) Hong, M. *J. Phys. Chem. B* **2007**, *111*, 10340–10351.
(64) Franks, W. T.; Zhou, D. H.; Wylie, B. J.; Money, B. G.; Graesser, D. T.; Frericks, H. L.; Sahota, G.; Rienstra, C. M. *J. Am. Chem. Soc.* **2005**, *127*, 12291–12305.
(65) Lorieau, J. L.; McDermott, A. E. *J. Am. Chem. Soc.* **2006**, *128*, 11505–11512.
(66) Lorieau, J. L.; Day, L. A.; McDermott, A. E. *Proc. Natl. Acad. Sci. U.S.A.* **2008**, *105*, 10366–10371.
(67) Yang, J.; Tasayco, M. L.; Polenova, T. *J. Am. Chem. Soc.* **2009**, *131*, 13690–13702.
(68) Chevelkov, V.; Fink, U.; Reif, B. *J. Am. Chem. Soc.* **2009**, *131*, 14018–14022.

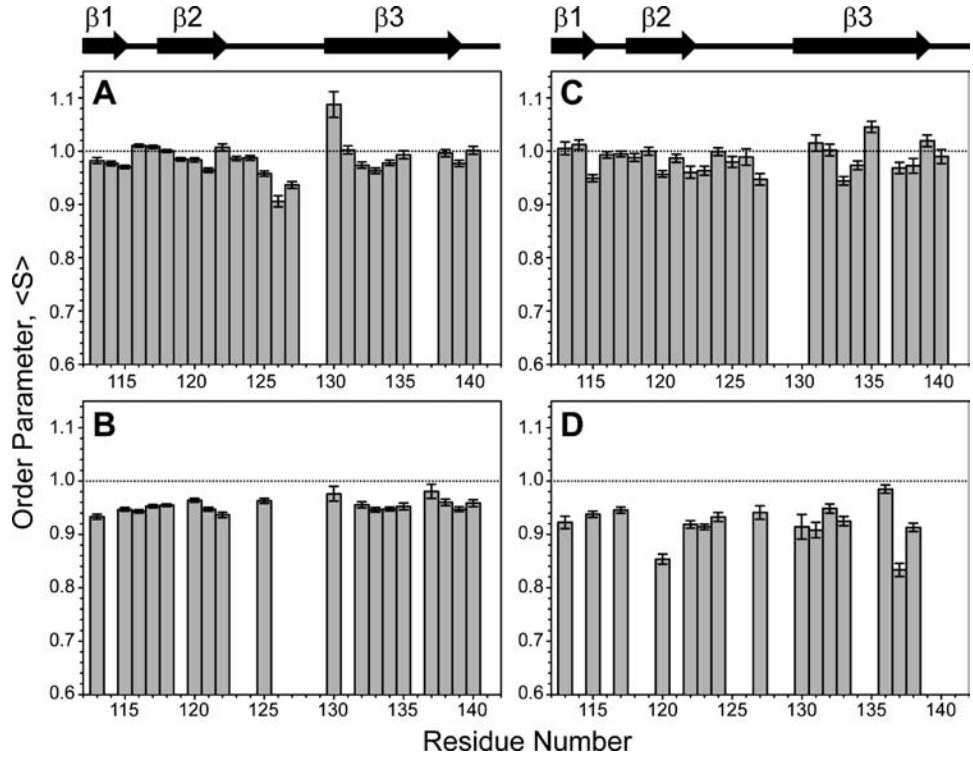

Figure 7. Backbone order parameters in the amyloid core region of huPrP23−144 fibrils derived from measurements of $^{1}H^{N}-^{15}N$ (A), $^{1}H^{\alpha}-^{13}C^{\alpha}$ (B), $^{15}N-^{13}C^{\alpha}$ (C), and $^{15}N-^{13}C'$ (D) one-bond dipolar couplings. The error bars correspond to $\pm 2\sigma$. Data points missing in the plots correspond to proline (A) and glycine (B) residues, and weak or overlapped correlations in 2D $^{15}N-^{13}C$ spectra. For each residue and coupling type, the order parameter is calculated as $\langle S \rangle = d_{IS}^{exp}/d_{IS}^{rigid}$, where d_{IS}^{exp} is the experimentally determined scaled dipolar coupling and d_{IS}^{rigid} is the corresponding dipolar coupling in the rigid-lattice limit. Bond lengths of 1.04 Å ($^{1}H^{N}-^{15}N$), 1.12 Å ($^{1}H^{\alpha}-^{13}C^{\alpha}$), 1.46 Å ($^{15}N-^{13}C^{\alpha}$), and 1.33 Å ($^{15}N-^{13}C'$), and pulse sequence dipolar scaling factors of 0.485 (T-MREV-4)[41] and 0.434 (TEDOR)[54] yield d_{IS}^{rigid} magnitudes of 5.25 kHz ($^{1}H^{N}-^{15}N$), 10.4 kHz ($^{1}H^{\alpha}-^{13}C^{\alpha}$), 427 Hz ($^{15}N-^{13}C^{\alpha}$), and 565 Hz ($^{15}N-^{13}C'$). Note that the $^{1}H^{N}-^{15}N$ and $^{1}H^{\alpha}-^{13}C^{\alpha}$ bond lengths used to calculate d_{IS}^{rigid} have been compensated for the effects of fast vibrational and librational averaging,[39,40,69−71] while the $^{15}N-^{13}C^{\alpha}$ and $^{15}N-^{13}C'$ bond lengths correspond to the standard crystallographic values.[72,73] See Table S2 for a summary of these calculations.

located in the non-β bend region between strands β1 and β2 and in the β3-strand, respectively. Additional dipolar trajectories are shown in Figures S4−S7, and the experimental dipolar coupling values extracted from these trajectories are summarized in Table S2.

The most remarkable feature of the data in Figure 6 is that, despite being associated with huPrP23−144 core residues that exhibit markedly different cross-peak intensities in CP-based SSNMR spectra (see Figure 4), the respective dipolar trajectories and, hence, dipolar order parameters for residues A117 and S132 appear to be nearly identical. This suggests the lack of major differences in submicrosecond time scale motions for these two sites. In fact, a complete analysis of the dipolar trajectories has enabled us to extend this conclusion to all huPrP23−144 amyloid core residues. In Figure 7, we show plots of the $^{1}H^{N}-^{15}N$, $^{1}H^{\alpha}-^{13}C^{\alpha}$, $^{15}N-^{13}C^{\alpha}$, and $^{15}N-^{13}C'$ dipolar order parameters as a function of residue number. These order parameters, which on average range from ∼0.92 ($^{15}N-^{13}C'$ couplings) to ∼0.98 ($^{1}H^{N}-^{15}N$ and $^{15}N-^{13}C^{\alpha}$ couplings) (see Table S2), indicate that not only are there no major differences in submicroseond time scale dynamics for residues located in different parts of the amyloid core but also that most residues are near the rigid-lattice limit on this time scale. Indeed, dipolar order parameters in this regime are reminiscent of well-structured regions of microcrystalline proteins,[64,65,67,68] and, within a motional model that describes dipolar vector dynamics as a restricted diffusion in a cone characterized by a semiangle α_0,[59,74] the observed $\langle S \rangle$ values correspond to motions with amplitudes of $\alpha_0 = \sim 10-20°$.

Transverse Nuclear Relaxation Rates of huPrP23−144 Amyloid Core Residues. Measurements of the backbone dipolar order parameters discussed above show that huPrP23−144 residues in the amyloid core region undergo rather limited and relatively uniform motions on the submicrosecond time scale. Such restricted dynamics do not lead to significant attenuation of the one-bond nuclear dipolar couplings and are therefore not able to account for the considerable variation of cross-peak intensities observed in CP-based SSNMR correlation spectra. Therefore, to further probe this issue, we have performed measurements of selected transverse relaxation rates for the backbone nuclei in the huPrP23−144 amyloid core region.

These measurements, which include rotating frame relaxation rates, $R_{1\rho}$, for $^{1}H^{N}$, ^{13}C, and ^{15}N nuclei, and the ^{15}N spin−spin relaxation rate, R_2, reveal considerable differences in magnitude for the various types of relaxation rate constants among the huPrP23−144 amyloid core residues. As an example, in Figure

(69) Henry, E. R.; Szabo, A. *J. Chem. Phys.* **1985**, *82*, 4753–4761.
(70) Ishii, Y.; Terao, T.; Hayashi, S. *J. Chem. Phys.* **1997**, *107*, 2760–2774.
(71) Roberts, J. E.; Harbison, G. S.; Munowitz, M. G.; Herzfeld, J.; Griffin, R. G. *J. Am. Chem. Soc.* **1987**, *109*, 4163–4169.
(72) Marsh, R. E.; Donohue, J. *Adv. Protein Chem.* **1967**, *22*, 235–256.
(73) Ramachandran, G. N.; Kolaskar, A. S.; Ramakrishnan, C.; Sasisekharan, V. *Biochim. Biophys. Acta* **1974**, *359*, 298–302.
(74) Lipari, G.; Szabo, A. *J. Am. Chem. Soc.* **1982**, *104*, 4546–4559.

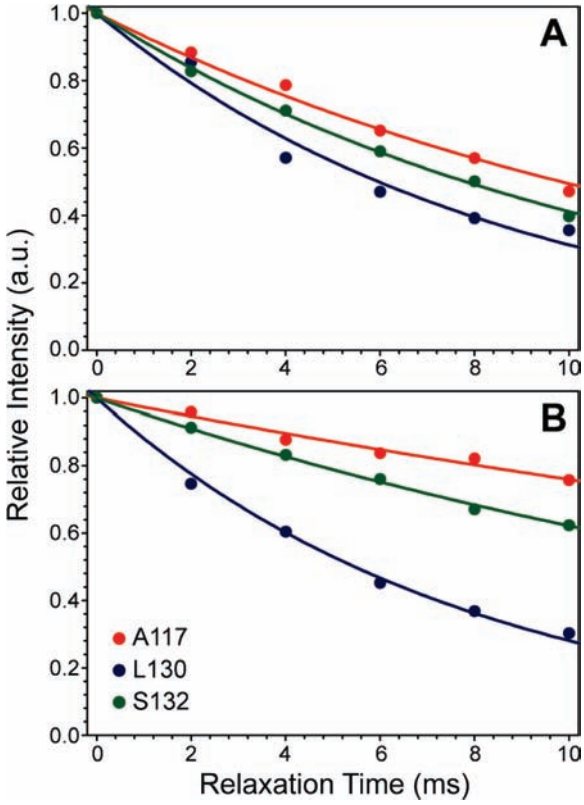

Figure 8. Selected site-resolved measurements of transverse relaxation rate constants, $R_{1\rho}$ and R_2, for residues in the amyloid core region of huPrP23−144 fibrils. $^1H^N$ $R_{1\rho}$ (A) and ^{15}N R_2 (B) trajectories, recorded using pulse schemes in Figure S3, are shown for residues A117, L130, and S132. Best-fit simulations to decaying single exponential curves are shown as solid lines. Additional $^1H^N$ $R_{1\rho}$, $^{13}C^\alpha$ $R_{1\rho}$, ^{15}N $R_{1\rho}$, and ^{15}N R_2 trajectories are shown in Figures S8−S11.

8 we show $^1H^N$ $R_{1\rho}$ and ^{15}N R_2 trajectories for residues A117, L130, and S132, which illustrate the sizable variations in relaxation behavior that can be observed on a site-specific basis. For this small subset of residues, the relaxation data are highly correlated with the relative cross-peak intensities obtained in CP-based SSNMR experiments (see Figure 4). Specifically, for A117, which exhibits relatively intense cross-peaks in multidimensional correlation spectra, the $^1H^N$ and ^{15}N nuclei are seen to relax relatively slowly. On the other hand, the same spins in L130 and S132 are associated with both increased transverse relaxation rates and significantly reduced cross-peak intensities relative to A117. A complete set of the residue- and site-specific transverse relaxation trajectories is presented in Figures S8−S11, and plots of the transverse relaxation rate constants as a function of residue number obtained by fitting the experimental relaxation trajectories to single exponential decays are shown in Figure 9. While considerable site-to-site fluctuations are evident for different types of relaxation rate constants for the huPrP23−144 amyloid core residues, with the exception of ^{15}N $R_{1\rho}$ rates, which are ∼50−60 s^{-1} and essentially invariant throughout the core region under the experimental conditions employed here, residues ∼115−120 consistently display relatively small relaxation rates, while larger $R_{1\rho}/R_2$ values (by as much as ∼50−100 s^{-1}) are observed, on the whole, for the C-terminal amino acids ∼130−141. These findings extend the conclusion made above for residues A117, L130, and S132 to the entire amyloid core region, in that the significant dispersion in relaxation rates of nuclear spin coherences is responsible for the large variation of cross-peak intensities in CP-based multidimensional SSNMR spectra of huPrP23−144 fibrils.

It is interesting to speculate here about the molecular level basis for the relatively large variations in certain types of transverse spin relaxation rates observed for the huPrP23−144 amyloid core residues. One possibility is that these variations are associated with different local densities of proton spins. This, however, appears to be rather unlikely, given that no consistent trends in relaxation rates are evident as a function of residue type or identities of the nearest neighbor residues. For example, a nearly 2-fold difference in ^{15}N R_2 is observed for glycines 114 and 119, both of which are flanked by alanine residues on either side. Another explanation relates to the presence of relatively slow, chemical exchange type phenomena, that occur in parts of the huPrP23−144 amyloid core region on the microsecond−millisecond time scale[59,60] and are thus undetectable via the dipolar order parameter measurements. Such processes, which would lead to the time-dependent modulation of chemical shifts and dipolar couplings, can potentially interfere with MAS and the applied RF fields leading to increased nuclear spin relaxation. While a definitive confirmation and quantitative description of motional phenomena of this type would require an extended series of SSNMR relaxation experiments[59,60] to be carried out on different types of isotopically labeled huPrP23−144 fibril samples and is beyond the scope of the current study, to provide a rough order-of-magnitude estimate of the time scale of processes that are consistent with the experimentally observed relaxation rate variations we have performed calculations of ^{15}N R_2 values using the theoretical spin−spin relaxation model presented by Rothwell and Waugh for the slow MAS regime[75] and subsequently extended to arbitrary MAS rates by Griffin and co-workers.[76] This model provides R_2 estimates for a simple system consisting of an isolated low-γ nucleus S (e.g., ^{13}C or ^{15}N) coupled to a single I-spin (^1H) and subject to MAS, ^1H continuous wave RF field, and random rotational diffusion of the I−S dipole−dipole interaction with a correlation time τ_c as follows:

$$R_2 = \frac{\omega_{IS}^2}{30}[2J(\omega_{RF} + \omega_r) + 2J(\omega_{RF} - \omega_r) + J(\omega_{RF} + 2\omega_r) + J(\omega_{RF} - 2\omega_r)] \quad (1)$$

where ω_{IS} is the $^1H-^{15}N$ dipolar coupling, ω_r is the MAS rate, ω_{RF} is the amplitude of the ^1H RF field (all in rad s^{-1}), and $J(\omega)$ is the spectral density function:

$$J(\omega) = \frac{\tau_c}{1 + \omega^2\tau_c^2} \quad (2)$$

Interestingly, these highly approximate calculations indicate that under the experimental conditions of this study molecular dynamics-related contributions to ^{15}N R_2 of ∼50−100 s^{-1}, which would be consistent with our experimental relaxation data (see Figure 9D), correspond to τ_c values in the ∼0.1−1 ms regime. Thus, the occurrence of nonuniform, microsecond−millisecond time scale chemical exchange phenomena within the huPrP23−144 amyloid core region, while far from being a direct proof, offers at least a plausible explanation for the experimen-

(75) Rothwell, W. P.; Waugh, J. S. *J. Chem. Phys.* **1981**, *74*, 2721–2732.
(76) Long, J. R.; Sun, B. Q.; Bowen, A.; Griffin, R. G. *J. Am. Chem. Soc.* **1994**, *116*, 11950–11956.

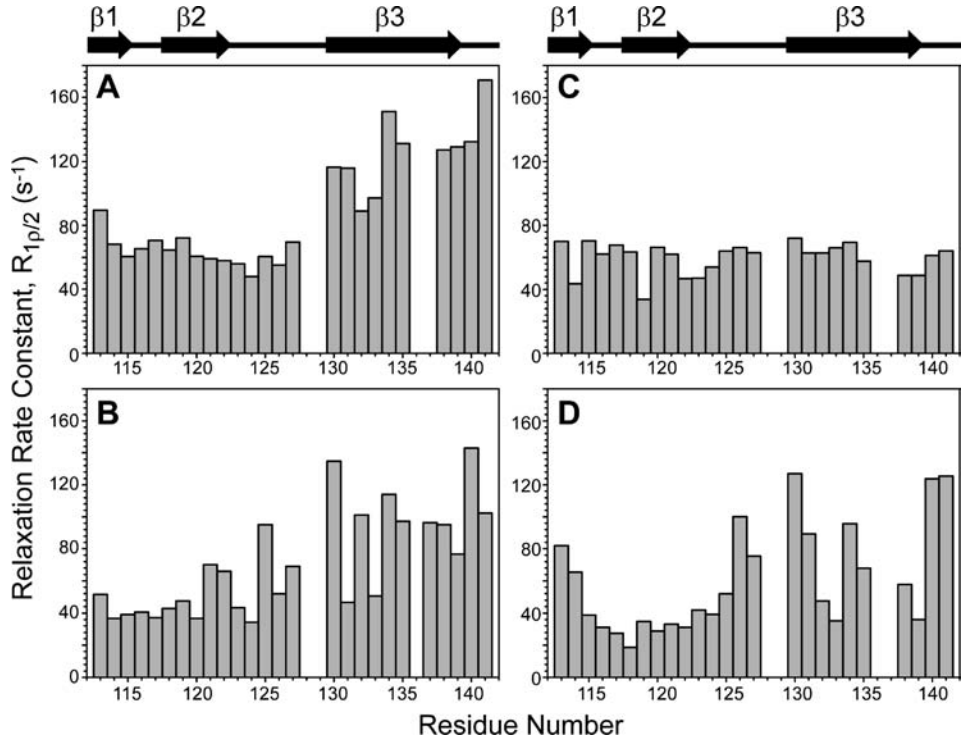

Figure 9. Site-specific $^{1}H^{N}$ $R_{1\rho}$ (A), $^{13}C^{\alpha}$ $R_{1\rho}$ (B), ^{15}N $R_{1\rho}$ (C), and ^{15}N R_2 (D) relaxation rate constants plotted as a function of residue number for the huPrP23−144 amyloid core region.

tally observed disparity in transverse nuclear spin relaxation rates.

Conclusions

In the present study, we have probed the conformational flexibility of the Y145Stop mutant of human prion protein in the amyloid state by using several types of magic-angle spinning solid-state NMR techniques. Two-dimensional solid-state NMR spectra based on *J*-coupling-driven magnetization transfers have permitted the direct observation, at ambient conditions, of N-terminal amino acid residues in the region ∼23−111, which are undetectable under the same conditions via conventional cross-polarization-based methods. Combined with the analysis of ^{1}H, ^{13}C, and ^{15}N isotropic chemical shifts for these residues, our results strongly suggest that the large N-terminal domain exists in huPrP23−144 fibrils as a highly dynamic ensemble of protein chains with random-coil-like conformations.

Remarkably, the core region of huPrP23−144 amyloid, although on the whole quite rigid in comparison to the N-terminal domain, appears to experience non-negligible molecular motions on the NMR time scale as well, implied by the considerable variation of signal intensities in CP-based solid-state NMR spectra. Our measurements of the backbone $^{1}H^{N}-^{15}N$, $^{1}H^{\alpha}-^{13}C^{\alpha}$, $^{15}N-^{13}C^{\alpha}$, and $^{15}N-^{13}C'$ dipolar order parameters for the core amino acids, which are observable in such spectra, reveal that these residues are reminiscent of well-structured regions of microcrystalline proteins and undergo only highly restricted and relatively uniform molecular motions on the submicrosecond time scale. On the other hand, significant dispersion in the relaxation rates of ^{1}H, ^{13}C, and ^{15}N nuclear spin coherences observed for the same huPrP23−144 core residues appears to be responsible for the large variation of spectral intensities. Although still somewhat speculative, the molecular basis of this finding is consistent with the presence of relatively slow, chemical exchange type phenomena taking place in this region of the protein on the microsecond−millisecond time scale. Interestingly, the results of our previous variable-temperature NMR studies[24] provide additional support for this chemical exchange hypothesis. Specifically, these experiments show that the most rigid amyloid core residues (aa 115−120) exhibit nearly identical resonance widths in 2D $^{15}N-^{13}C^{\alpha}$ correlation spectra recorded at 0 °C and upon freezing the sample at −30 °C, which indicates that these residues exist in huPrP23−144 fibrils in a single predominant conformation. In contrast, several core residues that are found in the C-terminal β3-strand and give rise to relatively well isolated signals in both 0 and −30 °C spectra, including S132, I138, and I139, display pronounced inhomogeneous linebroadening upon freezing the fibrils at −30 °C, consistent with the presence of several similar, but not identical, conformers for this region of the protein.

While for amyloid fibrils composed of short polypeptides the rigid amyloid core region typically encompasses the entire backbone and side-chains,[77−81] frequently within a steric-zipper type motif, analogous amyloid assemblies formed by intact protein molecules are, perhaps not surprisingly, far more complex. Indeed, the finding that Y145Stop human PrP amyloid fibrils contain both highly flexible large segments as well as a

(77) Sawaya, M. R.; Sambashivan, S.; Nelson, R.; Ivanova, M. I.; Sievers, S. A.; Apostol, M. I.; Thompson, M. J.; Balbirnie, M.; Wiltzius, J. J.; McFarlane, H. T.; Madsen, A. Ø.; Riekel, C.; Eisenberg, D. *Nature* **2007**, *447*, 453–457.
(78) Jaroniec, C. P.; MacPhee, C. E.; Bajaj, V. S.; McMahon, M. T.; Dobson, C. M.; Griffin, R. G. *Proc. Natl. Acad. Sci. U.S.A.* **2004**, *101*, 711–716.
(79) Nadaud, P. S.; Sarkar, M.; Wu, B.; MacPhee, C. E.; Magliery, T. J.; Jaroniec, C. P. *Protein Expression Purif.* **2010**, *70*, 101–108.
(80) van der Wel, P. C. A.; Lewandowski, J. R.; Griffin, R. G. *J. Am. Chem. Soc.* **2007**, *129*, 5117–5130.
(81) Madine, J.; Jack, E.; Stockley, P. G.; Radford, S. E.; Serpell, L. C.; Middleton, D. A. *J. Am. Chem. Soc.* **2008**, *130*, 14990–15001.

relatively rigid, well-structured core domain that overall exhibits more restricted motions on different time scales appears to be general in nature, as similar observations have been made for several other protein-based amyloid structures that have been investigated to date in atomic-level detail.[26−32,82] Interestingly, the concurrent presence of such rigid and flexible protein domains is quite consistent with the initial molecular models of amyloid fibrils,[83] where the packing of individual protein monomers into an amyloid scaffold was presumed to be generally associated with substantial rearrangements of the native protein fold to yield a compact β-sheet core flanked by other types of structural motifs. We note, however, that the existence of amyloid architectures consisting of protein molecules in a native-like conformation has also been recently reported,[84] further underlining the structural and dynamic complexities intrinsic to these types of biomacromolecular assemblies. The fundamental insights into the dynamic properties of human PrP23−144 amyloid obtained in this study should facilitate future efforts aimed at the full understanding of the molecular basis of amino acid sequence- and strain-dependent conformational inheritance in this biologically relevant in vitro model.[22,23] Questions in this regard are of central importance in prion and amyloid research.

Acknowledgment. This work was supported by grants from the National Science Foundation (CAREER Award MCB-0745754 to C.P.J.) and the National Institutes of Health (NS-44158 and NS-38604 to W.K.S.), and Eli Lilly and Co. (Young Investigator Award to C.P.J.).

Supporting Information Available: Complete refs 19 and 57; figures with pulse sequences and additional dipolar coupling and relaxation trajectories; tables of ^{1}H and ^{13}C resonance assignments for flexible huPrP23−144 residues, and dipolar couplings and order parameters for amyloid core residues. This material is available free of charge via the Internet at http://pubs.acs.org.

JA909827V

(82) Toyama, B. H.; Kelly, M. J.; Gross, J. D.; Weissman, J. S. *Nature* **2007**, *449*, 233–237.
(83) Jimenez, J. L.; Guijarro, J. I.; Orlova, E.; Zurdo, J.; Dobson, C. M.; Sunde, M.; Saibil, H. R. *EMBO J.* **1999**, *18*, 815–821.
(84) Loquet, A.; Bousset, L.; Gardiennet, C.; Sourigues, Y.; Wasmer, C.; Habenstein, B.; Schütz, A.; Meier, B. H.; Melki, R.; Böckmann, A. *J. Mol. Biol.* **2009**, *394*, 108–118.